13th World Conference on Earthquake Engineering
Vancouver, B.C., Canada
August 1-6, 2004
Paper No. 350

STABILITY ANALYSIS OF THE PERMANENT SHIPLOCK SLOPES OF THE TGP UNDER SEISMIC ACTION

Jian CHEN[1], Jian-Hua YIN[1]*, and and C. F. LEE[2]

SUMMARY

The stability of the permanent shiplock slopes is among the key issues in the design and construction of the Three Gorges Project. The attention of this paper is paid to the stability analysis of the permanent shiplock slopes under the seismic action. The seismic load is considered as a quasi-static force, and the stability analysis of the slopes is carried out by means of an upper bound limit analysis based on rigid elements. The problem of finding the minimum value of the critical seismic coefficient can be set up as a linear programming problem and solved by a revised simplex method.

INTRODUCTION

The Three Gorges Project (TGP), currently under construction, is the largest water conservancy project in China and is of vital importance to the sustainable development of the Yangtze River delta region. The permanent shiplock, a double-line continuous five-stage flight structure with a total chamber length of 1607m, has been constructed by excavating deeply and widely into the mountain on the north bank of the Yangtze River. As a result of such excavation, the permanent cut slopes in both weathered and fresh granitic rocks have been formed. The slopes comprise two steep upper cut slopes and four vertical ones. A 60m wide central rock barrier is kept between the north and the south chambers, as shown in Fig. 1. The maximum height of the cut slope is about 170m. The unloading process due to such large scale excavation would definitely have some negative effects on the mechanical properties of the rock mass in the permanent slopes. The stability of the permanent shiplock slopes after excavation and during operation is among the key issues of the TGP, having drawn considerable interest from the geotechnical communities in China and around the world. Many relevant researches based on different approaches, such as field investigation, in-situ test, physical and numerical simulation, displacement back analysis and so on, has been carried out, and a number of achievement have been obtained [1-4].

This paper employs the pseudo-static approach combined with a rigid-element-based upper bound limit analysis to evaluate the two-dimensional stability of the permanent shiplock high slopes under the seismic action. In a pseudo-static analysis, the effect of the actual time history of the response of the slope to the earthquake and other time-dependent phenomena has been neglected. The seismic stability of the slope is expressed in terms of a single parameter, the critical seismic coefficient, k_c. This coefficient is

[1] Department of Civil & Structural Engineering, The Hong Kong Polytechnic University, Hong Kong
[2] Department of Civil Engineering, The University of Hong Kong, Hong Kong

the ratio of the seismic acceleration, a_c, yielding a factor of safety equal to unity, to the acceleration of gravity g. The seismic acceleration is usually assumed to be horizontal. In this study, it was assumed that the soil and rock follow the Mohr-Coulomb yield criterion, and the seismic coefficient has the same value throughout the slope.

ROCK MASS PROPERTIES

The permanent shiplock slopes comprise amphibole-plagioclase granite, which is generally sound and intact with a very limited distribution of schist xenoliths and veins. The granite is completely decomposed at the ground surface. The degree of weathering decreases with an increase in depth, until reaching the fresh rock. Based on the type and macrostructure of the rock block, the integrity and mechanical properties of the rock mass, and the hydrologic properties, four different grades of weathering in the granite are identified as follows (shown in Figure 1): (a) slightly weathered and fresh (I); (b) moderately weathered (II); (c) heavily weathered (III); and (d) completely weathered rock (IV). The moderately weathered granite can be further subdivided into an upper part (II2) and a lower part (II1), based on the differences in weathering characteristics and engineering geologic properties.

Faults are uncovered on the vertical sidewalls of the shiplock chambers and the upper surface of the central rock barrier. In the central barrier and southern slopes, the fault set with the strike direction of north to northwestern (NNW) is the most highly developed, followed by the set with direction of northeastern to east (NEE). While in the northern slopes, the NEE fault set is the most developed, followed by the NNW and NNE (north to northeastern) fault sets.

For the purpose of design and numerical analysis, the values of the mechanical properties of the granites and faults have been summarized in Table 1, based on the geological investigation and in-situ test.

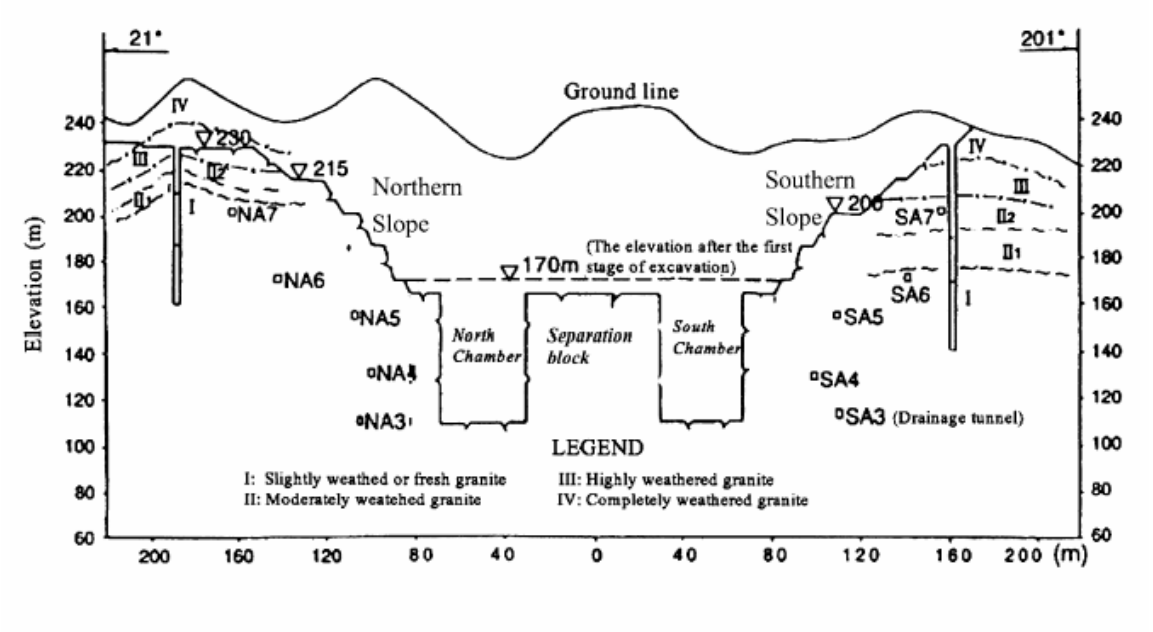

Figure 1. Typical cross-section of the permanent shiplock chambers

Table 1. Parameters of granites and faults adopted in numerical analysis

Rock type	I	II	III	IV	Fault
Unit weight (kN/m^3)	27.0	26.8	26.5	26.5	26.5
Young's modulus (10^3kN/m^2)	40.0	15.0	1.0	1.0	5.0
Poisson's ratio	0.22	0.24	0.30	0.30	0.35
Cohesion (kN/m^2)	1.8	1.0	0.35	0.35	0.5
Friction angle (^{o})	60.9	52.4	45.0	45.0	45.0

UPPER BOUND LIMIT ANALYSIS USING RIGID ELEMENTS

Rigid Element Discretization

The rigid element method (REM) is originated from the rigid body-spring model (RBSM) proposed by Kawai [5] and has been extended by Qian and Zhang [6, 7]. REM provides an effective approach to the numerical simulation of the stability of soils or rocks or discontinuous media. In this method, each element is assumed rigid, and only the relative sliding between adjacent elements is taken into account. The displacements (velocities) of any point in a rigid element can be described as a function of the translation and rotation of the element centroid. The deformation energy of the system is stored only in the interfaces between the rigid elements.

Any point in 2-D case has two degrees of freedom, the x and y velocities, normally denoted v_x and v_y. Each rigid element is associated with a three-dimensional vector $\mathbf{V}_g$ of velocity variables at its centroid, that is, the rigid element has both translational v_{xg} and v_{yg}, and rotational $v_{\omega g}$. The velocity $\mathbf{V}$ of any point P(x, y) at an interface in the global coordinate system can be written as

$$\mathbf{V} = \mathbf{N}\mathbf{V}_\mathbf{g} \tag{1}$$

where

$$\mathbf{V} = \begin{bmatrix} v_x & v_y \end{bmatrix}^T \tag{2}$$

$$\mathbf{V}_\mathbf{g} = \begin{bmatrix} v_{xg} & v_{yg} & v_{\omega g} \end{bmatrix}^T \tag{3}$$

$$\mathbf{N} = \begin{bmatrix} 1 & 0 & y_g - y \\ 0 & 1 & x - x_g \end{bmatrix} \tag{4}$$

It should be pointed out here that in order to ensure the application of the upper bound theorem, there must be no gap or overlap occurring anywhere in the soil mass. One approach to do this is to set the rotation at the centroid of each element as zero so as to make the velocity field kinematically feasible and therefore to give an upper bound solution. Another promising approach is to enforce the flow rule at two points along the discontinuity (e.g. at its end ends) so that solution is kinematically admissible with rotations. In this study, we set the rotations of each element centroid as zero, that is, $v_{\omega g} = 0$. Only the relative sliding between adjacent elements is taken into account in present upper bound method. The work related to the enforcement the flow rule at two points will be carried out in future.

Figure 2 shows two triangular elements (1) and (2) with global velocities $\mathbf{V}^{(1)}$ and $\mathbf{V}^{(2)}$ respectively (magnitude denoted as $v^{(1)}$ and $v^{(2)}$) at a point P. The point P on the interface of Element (1) moves at velocity $\mathbf{V}^{(1)}_{local}$, and the same point on the interface of Element (2) moves at velocity $\mathbf{V}^{(2)}_{local}$. The two

velocities $\mathbf{V}_{local}^{(1)}$ and $\mathbf{V}_{local}^{(2)}$ take the same local coordinate axes at the interface on Element (1) as the reference system. The relative velocity jump can be expressed as $\mathbf{\Delta V}_{local}^{(2-1)} = \mathbf{V}_{local}^{(2)} - \mathbf{V}_{local}^{(1)}$. Using the local n-s coordinate system, the relative velocity $\mathbf{\Delta V}_{local}^{(2-1)}$ at point P can be decomposed into two components: in the normal direction by Δv_n, and in the strike direction by Δv_s, that is, $\mathbf{\Delta V}_{local}^{(2-1)} = [\Delta v_n, \Delta v_s]^T$.

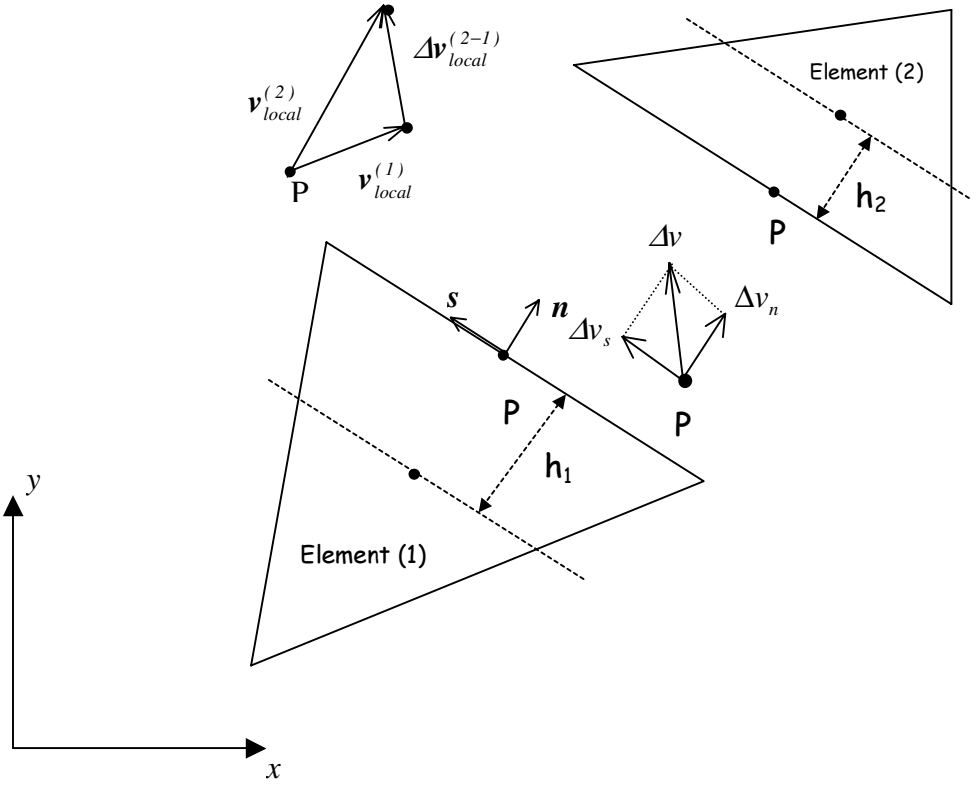

Figure 2. 2-D velocity discontinuity

For convenience, we denote $\mathbf{\Delta V}_{local}^{(2-1)}$ as $\mathbf{\Delta V}$ in the rest of this chapter. The relative velocity jump at point P expressed in terms of the velocities in the local coordinate system can be then expressed by the velocities $\mathbf{V}^{(1)}$ and $\mathbf{V}^{(2)}$ in the global coordinate system:

$$\mathbf{\Delta V} = \mathbf{L}^{(1)}\mathbf{V}^{(2)} - \mathbf{L}^{(1)}\mathbf{V}^{(1)} \tag{5}$$

$$\mathbf{L}^{(1)} = \begin{bmatrix} \cos(\mathbf{n},\mathbf{x}) & \cos(\mathbf{n},\mathbf{y}) \\ \cos(\mathbf{s},\mathbf{x}) & \cos(\mathbf{s},\mathbf{y}) \end{bmatrix} \tag{6}$$

where $\mathbf{L}^{(1)}$ is the matrix of direction cosines of the local n-s axes on the interface of Element (1) with respect to the global coordinate system.

Using Equation (1) for the global velocity $\mathbf{V}_g$ at the element centroid, Equation (5) can be written as

$$\mathbf{\Delta V} = \mathbf{L}^{(1)}(\mathbf{N}^{(2)}\mathbf{V}_g^{(2)} - \mathbf{N}^{(1)}\mathbf{V}_g^{(1)}) \tag{7}$$

Equation (7) can be given in a compact form

$$\mathbf{\Delta V} = \mathbf{A}_1\mathbf{V}_G \tag{8}$$

where

$$\mathbf{A}_1 = \begin{bmatrix} \mathbf{L}^{(1)} & -\mathbf{L}^{(1)} \end{bmatrix} \begin{bmatrix} \mathbf{N}^{(2)} & \mathbf{0} \\ \mathbf{0} & \mathbf{N}^{(1)} \end{bmatrix} \tag{9}$$

$$\mathbf{V_G} = \begin{Bmatrix} \mathbf{V}_g^{(2)} \\ \mathbf{V}_g^{(1)} \end{Bmatrix} \tag{10}$$

Constraints at Velocity Discontinuities

Velocity discontinuities are allowed to occur at any edge that is shared by a pair of adjacent triangles. In order to be kinematically admissible, the velocity discontinuities must satisfy a plastic flow rule. According to the Mohr-Coulomb failure criterion (or yield criterion for perfect plasticity) and the associated flow rule, the relationship between the normal velocity magnitude (Δv_n) and tangential velocity magnitude (Δv_s) jumps across the discontinuity can be written as

$$\Delta v_n = -\left|\Delta v_s\right| \tan\phi' \tag{11}$$

The existence of the absolute value sign on the right hand side of Equation (11) makes it difficult to derive a set of flow rule constraints that are everywhere differentiable. It is clear that Δv_s may be zero, negative or positive. From the mathematic programming point of view, this is referred to as an unrestricted-in-sign variable. Any unrestricted quantity can be decomposed into the difference of two non-negative quantities. Thus, the tangential velocity jump Δv_s defined in the local n-s coordinate system can be decomposed into two non-negative variables v^+ and v^-

$$\Delta v_s = v^+ - v^- \tag{12}$$

with the constraints

$$\begin{aligned} v^+ &\geq 0 \\ v^- &\geq 0 \end{aligned} \tag{13}$$

In order to remove the absolute value sign, and thus the equation can be set into a standard mathematic programming problem, we follow the formulation derived by Sloan et al. [8, 9]. Hence $|\Delta v_s|$ is replaced by

$$\left|\Delta v_s\right| = v^+ + v^- \tag{14}$$

Therefore, the tangential velocity jump is automatically determined by finding the values of a pair of unknown variables v^+ and v^-, without any sign restrictions, during the computation process. And the normal velocity jump is therefore given by

$$\Delta v_n = -(v^+ + v^-)\tan\phi' \tag{15}$$

In matrix notation, equations (12) - (15) can be written as

$$\begin{aligned} \mathbf{\Delta V} &= \mathbf{A}_2 \mathbf{V_d} \\ \mathbf{V_d} &\geq 0 \end{aligned} \tag{16}$$

where

$$\mathbf{A}_2 = \begin{bmatrix} -\tan\phi' & -\tan\phi' \\ 1 & -1 \end{bmatrix} \tag{17}$$

$$\mathbf{V_d} = \{v^+, v^-\}^T \tag{18}$$

Velocity Boundary Conditions

As stated in the upper bound theorem, the computed velocity field must satisfy the prescribed velocity boundary conditions. Considering Element k on a boundary where the imposed velocity is $\overline{\mathbf{V}}$, the element velocity $\mathbf{V}_g^k$ must satisfy the following equality

$$\mathbf{V}_g^k = \overline{\mathbf{V}} \tag{19}$$

Energy-work Balance Equation

The upper bound theorem is based on the principle of virtual work. The limit load or factor of safety is determined by equating the internal rate of energy dissipation and the rate of work by external forces. While applying to the soil stability problems using the REM, the virtual work equation, often termed "the energy-work balance equation", can be expressed mathematically as

$$\int_{\Omega^*} \sigma'_{ij} \dot{\varepsilon}^*_{ij} d\Omega^* + \int_{\Gamma^*} \sigma'_{\Gamma^*} \dot{\varepsilon}^*_{\Gamma^*} d\Gamma^* = \boldsymbol{W}\boldsymbol{V}^* + k_c \boldsymbol{W}\boldsymbol{V}^* \tag{20}$$

The first term in the left-hand side in Equation (20) is the rate of work done by the effective stress σ'_{ij} over the virtual strain rates $\dot{\varepsilon}^*_{ij}$, dissipated within Ω*. The second left-hand side term is the rate of the internal energy dissipation along the slip surface and discontinuities Γ*. The right-hand side terms in Equation (20) represent the rate of external work done by the self-weight of the sliding mass W and horizontal seismic acceleration over the virtual velocity V*.

In the present kinematical approach, according to the rigid assumption for the elements, there is no energy dissipation within elements. Thus the first term on the left-hand side of Equation (20) equals zero, that is, $\int_{\Omega^*} \sigma'_{ij} \dot{\varepsilon}^*_{ij} d\Omega^* = 0$. The energy is dissipated only along the failure surface and the interfaces between the elements. The energy dissipated along the failure surface and the interfaces by normal and tangential stresses can be expressed by the following equation

$$\int_{\Gamma^*} \sigma'_{\Gamma^*} \dot{\varepsilon}^*_{\Gamma^*} d\Gamma^* = \int_{S_d} (|\tau \Delta v_s| - \sigma'_n \Delta v_n) dS \tag{21}$$

Using the Mohr-Coulomb yield criterion and the associated flow rule in Equation (11), the right hand side in Equation (21) can be replaced as

$$\int_{S_d} (|\tau \Delta v_s| - \sigma'_n \Delta v_n) dS = \int_{S_d} c' |\Delta v_s| dS = \int_{S_d} c' (v^+ + v^-) dS \tag{22}$$

As can be seen, Equation (22) does not involve any stress calculations. It indicates that the rate of energy dissipation based on the Mohr-Coulomb criterion can be conveniently calculated without the knowledge of the stresses while using the REM. It is a simple matter to calculate the lengths of the lines of discontinuity. The rate of energy dissipation is then found by multiplying the length of each discontinuity line by c times the velocity jump across the line, and summing over all such lines.

The rate of external work done by soil weight and horizontal seismic acceleration is found by multiplying the corresponding load times by the velocity of each related rigid element and summing over all the domains in motion.

Using Equation (22), the energy-work balance equation can be approximated in the form of a summation

$$\sum_{i=1}^{n_D} \mathrm{c}'_{\mathrm{i}} \mathrm{l}_{\mathrm{i}} (v_i^+ + v_i^-) = \boldsymbol{W}\mathbf{V}_{\mathbf{g}} + k_c \boldsymbol{W}\mathbf{V}_{\mathbf{g}} \tag{23}$$

With the conservative assumption that the effective cohesion *c'* and frictional angle ϕ' at the discontinuity between elements do not exceed the effective cohesion and frictional angle of the weakest soil in the adjacent elements, Equation (23) can be written in the following general matrix form

$$\mathbf{A}_3\mathbf{V}_d = \mathbf{A}_4\mathbf{V}_g \tag{24}$$

where

$$\mathbf{A}_3 = \{c_i^{'} l_i\}^T \qquad i = 1,...,n_D \tag{25}$$

$$\mathbf{A}_4 = \boldsymbol{W} + k_c\boldsymbol{W} \tag{26}$$

$c_i^{'}$ is cohesion in terms of effective stress at discontinuity i shared by two adjacent elements, l_i is the length of the discontinuity i, and n_D is the total number of discontinuities.

Assembly of Constraint Equations

All of the steps that are necessary to formulate the upper bound theorem as an optimisation problem have now been covered. The task of finding a kinematically admissible velocity field that minimizes the factor of safety may be stated as

$$\text{Minimize} \quad k_c$$

$$\text{Subject to} \quad \begin{cases} \mathbf{A}_1\mathbf{V}_G = \mathbf{A}_2\mathbf{V}_d \\ \mathbf{A}_3\mathbf{V}_d = \mathbf{A}_4\mathbf{V}_g \\ \mathbf{V}_g^k = \overline{\mathbf{V}} \\ \mathbf{V}_d \geq 0 \end{cases} \tag{27}$$

Therefore, finding the least critical seismic coefficient can be set into a linear programming problem. The complete constraint matrix is a sparse matrix with more unknowns than constraints. Such problem can be solved efficiently by the revised simplex method [10].

In order to obtain the static factor of safety F, the strength parameters of the material along the slip surface must be reduced by a known factor of safety and the critical acceleration computed. The value of the factor which gives zero critical acceleration is the factor of safety which obtains without the earthquake forces.

CALCULATION RESULTS

Figure 3 shows the mesh of the southern slope in the cross-section No. 16-16 for the upper bound calculations. The obtained values of critical seismic acceleration and factor of safety are presented in Table 2. It can be seen under seismic action, the factor of safety are all larger than 1.0. It also can be seen that the computed factors of safety of the northern slope are much higher than those of the corresponding southern slope in both two sections. In general, the shiplock slopes are stable.

Table 2. Calculated factors of safety

Cross-section	16-16		20-20	
	k_c	F	k_c	F
Northern slope	0.715	3.611	0.524	2.364
Southern slope	0.172	1.455	0.156	1.326

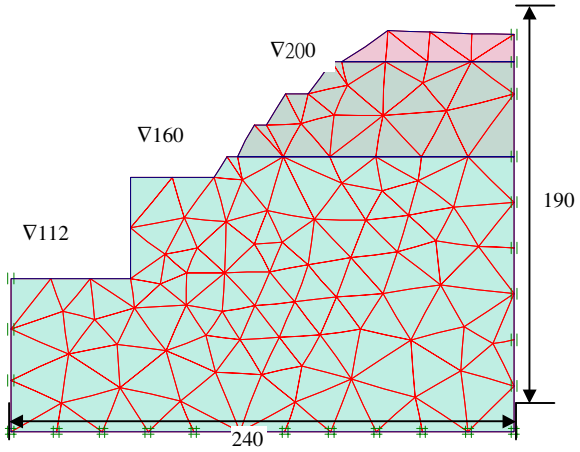

Figure 3. Geometry model and mesh

CONCLUSIONS

Stability analysis of the high slopes of the permanent shiplock in TGP under the effects of seismic action has been carried out using rigid-element-based upper bound limit analysis in conjunction with a pseudo-static approach.

- The factors of safety obtained from upper bound limit analysis are larger than 1.0. This confirms the adequacy of the geological condition for ensuring overall stability of the permanent shiplock slopes.
- Upper bound limit analysis can handle complicated cases (complex slope geometry, soil profiles, loading conditions, and material properties) efficiently and with relative ease.

REFERENCES

1. Chen, D.J. 1999. Engineering geological problems in the Three Gorges Project on the Yangtze, China. *Engineering Geology* 51(3): pp.183-193.
2. Feng, X.T., Zhang, Z.Q. & Sheng, Q. 2000. Estimating mechanical rock mass parameters for the Three Gorges permanent shiplock using an intelligent displacement back analysis method. International Journal of Rock Mechanics & Mining Sciences 37(7): pp.1039–1054.
3. Deng, J.H. & Lee, C.F. 2001. Displacement back analysis for a steep slope at the Three Gorges Project site. *International Journal of Rock Mechanics & Mining Sciences* 38(2): pp.259–268.
4. Sheng, Q, Yue, Z.Q, Lee, C.F., Tham, L.G. & Zhou, H. 2002. Estimating the excavation disturbed zone in the permanent shiplock slopes of the Three Gorges Project, China. *International Journal of Rock Mechanics & Mining Sciences* 39(2): pp.165-184.
5. Kawai, T. 1977. New discrete structural models and generalization of the method of limit analysis. *Finite Elements in Nonlinear Mechanics*. NIT, Tronheim. pp.885-906.
6. Zhang, X. & Qian, L.X. 1993. Rigid finite element and limit analysis. *Acta Mech Sinica* (English Edition) 9(2): pp.156-162.

7. Qian, L.X. & Zhang, X. 1995. Rigid finite element method and its applications in engineering. *Acta Mech Sinica* (English Edition) 11(1): pp.44-50.

8. Sloan, S.W. & Kleeman, P.W. 1995. Upper bound limit analysis using discontinuous velocity fields. *Computer Methods in Applied Mechanics and Engineering*.127: pp.293-314.

9. Lyamin, A.V. & Sloan, S.W. 2002. Upper bound limit analysis using linear finite elements and non-linear programming. *International Journal for Numerical and Analytical Methods in Geomechanics* 26(2): pp.181-216.

10. Best MJ, Ritter K. 1985. *Linear programming: Active set analysis and computer programs.* Prentice-Hall: Englewood Cliffs.